Solvent Effects on the Structure of Petroleum Asphaltenes

Yuan Yang[†], Thomas F. Headen[‡], Jingzhou Zhang[†], and Michael P. Hoepfner^{†*}

- † Department of Chemical Engineering, The University of Utah, 50 South Central Campus Drive, Salt Lake City, LTT 84112
- ‡ ISIS Pulsed Neutron and Muon Source, Rutherford Appleton Laboratory, Harwell Oxford, Didcot OX11 0QX, UK
- *Contact: michael.hoepfner@utah.edu

ABSTRACT

Neutron total scattering was employed to study the impact of solvent on the behavior of asphaltenes by comparing structural interpretations of solid phase samples to those dispersed in 1-methylnaphthalene (1-MN) as a function of temperature and asphaltene solubility. This powerful technique enables structural interpretation on length scales ranging from local molecular order to the formation of nanoaggregates and/or fractal clusters in a single experiment. We observed that more unstable asphaltenes exhibit greater aromatic stacking on the local molecular length scale and also produce more frequent nanometer-sized associations. However, when the temperature was elevated, the breakup of larger asphaltene clusters was correlated to a reduction in the extent of asphaltene sidechain interactions. Additionally, dispersed asphaltenes demonstrated an increase in aromatic stacking as the temperature was increased, suggesting an entropic driving-force for assembly driven by solvent depletion interactions. This observation is novel in asphaltene science and serves a pathway to assess the impact of local solvent composition on both enthalpic and entropic assembly pathways. The results suggest that while more unstable asphaltenes exhibit greater aromatic stacking, further association may be assisted by an increase in the disordered side-chain interactions. The experimental results also serve as a useful benchmark to validate simulation predictions of asphaltene structure.

1. Introduction

While petroleum asphaltenes have been extensively investigated for over 100 years, ^{1–7} there remains deep uncertainty about their molecular structure ^{2,3,8–10} and self-association, ^{9,11–14} hence the potential for understanding function through structure remains distant. ^{15–18} Petroleum asphaltenes are functionally defined as the material in crude oil that is insoluble in n-alkanes but soluble in aromatic solvents. ^{19–23} They are generally characterized as the most aromatic and densest fraction of crude oil. Understanding asphaltene phase behavior, precipitation mechanisms, and transport properties are critical to designing prevention and remediation strategies to several industrial process concerns (e.g., wellbore deposition). ^{10,11,23,24} Due to the compositional complexity and polydispersity of petroleum, ^{2,3,10,11,25,26} there will be mixtures of compounds on opposite ends of the distribution of chemical properties that are only marginally soluble in each other. Consequently, changes in the thermodynamic state of petroleum (e.g., temperature, pressure and composition) can alter the delicate balance of crude oil and cause asphaltenes to precipitate. ^{23,27}

The conventional understanding of asphaltene self-assembly is that the predominantly planar aromatic cores of asphaltenes stack into disc-like aggregates call "nano-aggregates" (aggregates of 5-8 molecules with a radius less than 5 nm). ^{2,3,10,11} Nano-aggregates further associate into fractal clusters with larger sizes (radius of gyration, R_g, less than approx. 40 nm) and a loose internal structure (i.e., extensively solvated) in good solvents and crude oil. ^{14,28} Previous studies demonstrate that asphaltenes fall into the category of "soft matter" where their assembled structures could be altered by liquid surroundings or thermodynamic conditions, similar to liquid crystals, polymers, etc. ^{10,11,29} The fractal cluster structure of asphaltenes has been extensively studied in the liquid phase using small-angle scattering (SAS)^{11,29–31} and transport measurements. ^{32–34} The solvent environment is expected to affect the shape and size of the fractal clusters and can result in the precipitation/dissociation of asphaltene clusters. ¹¹ Further, the length-scale of fractal association has been inversely correlated to the stability

of asphaltenes in solvent mixtures (i.e., larger clusters are less stable)^{10,11} and stands as an opportunity for the prediction of asphaltene phase behavior.

The influence of the liquid surroundings on the larger asphaltene structures (e.g., fractal clusters) is commonly studied in toluene and toluene-heptane systems, 9,10 while the nano-aggregate structure at the molecular length-scale has rarely been investigated in the liquid phase. Prior work has nearly exclusively attempted to gain insight into this process by extracting asphaltenes from the liquid and performing X-ray diffraction or other analytical approaches (e.g., nuclear magnetic resonance, NMR) on the solid precipitate. ^{2,8,28,35} These studies revealed that the asphaltenes molecules consist of an aromatic structure along with alkyl side chains, and nano-aggregates are formed by the stacking of the aromatic regions. Solid phase NMR experiments demonstrate that the alkyl side chains of asphaltenes contribute significantly to their overall intermolecular structure, further complicating the intermolecular structure of asphaltene associations. 35 Beyond the extensive studies on the solid phase, there is limited information of the self-association of asphaltenes into nano-aggregates in the liquid phase, save for a few recent wide-angle X-ray scattering (WAXS) studies. 10,36 Previous research suggests that changes in the dilution concentration or temperature only modify the overall size and weight of the clusters, instead of the shape or internal structure (fractal dimension) of the clusters. 10,11 The variance in the fractal dimension of clusters is likely related to the interaction between nanoaggregates. Therefore, local structural changes in nano-aggregates are hypothesized to affect anisotropic self-assembly³⁷ mechanisms and modify the stability of asphaltene clusters. Previous WAXS measurements¹⁰ showed that the molecular ordering of nano-aggregates in the liquid phase is altered by different solvents. Therefore, a multi-scale investigation of the liquid phase structure of asphaltenes ranging from the cluster to molecular length-scales sheds light onto the mechanistic effect of solvent on asphaltene structure and phase behavior. Additionally, details on the molecular structure

of asphaltenes from differing sources may be inferred from the self-assembly properties when experimental diffraction results are paired with molecular-level modeling.

Neutron total scattering has been extensively applied to measure the intermolecular structure of liquids using a combination of experimental isotopic substitution (e.g., H₂O to D₂O) and computational tools for molecular refinement (e.g., Empirical Potential Structural Refinement, EPSR).³⁹ As an example, the arrangement of the atoms in water has been extensively investigated by using neutron diffraction. 38,39 As neutrons interact with hydrogen (H) and deuterium (D) in different ways, isotopic substitution is widely used by selectively replacing H with D in a molecule to distinguish different groups in neutron diffraction results. 40,41 However, only recently have these tools been applied to organic liquids (e.g., benzene and naphthalene). 42,43 Using H/D substitution and EPSR to refine an atomistic simulation against experimental scattering data, an ensemble average of the full 3D structure of a fluid can be obtained to understand the intermolecular geometry of the system. 42,43 Asphaltene nano-aggregates are typically depicted in schematics as having well-ordered stacking of the polyaromatic cores; however, the extent of this specific type of interaction is poorly understood when dispersed in a liquid. For benzene, a perpendicular intermolecular geometry (Y-shaped) is preferentially observed compared to parallel π - π type stacking. For naphthalene, the opposite geometry is found and the parallel π - π type stacking is significantly more dominant than perpendicular structures. 42,43 Atomistic molecular dynamics simulations using the OPLS-AA force field reproduce the general trends of naphthalene liquid structure but fail to capture the extent of π - π type stacking in naphthalene accurately. Ideally, one would like to obtain similar detailed conclusions of the intermolecular structure of asphaltenes; however, the system heterogeneity prevents identical analysis. As an alternative, this report details experiments comparing the local intermolecular structure to fractal cluster formation and bulk phase behavior.

The advantage of scattering is that the expected scattering profile can be directly generated based on the positions of molecules from an atomistic simulation. Consequently, experimental diffraction data can be directly used to evaluate the accuracy of molecular simulations to provide valuable insight into the inter/intra-molecular structure of asphaltenes in liquid systems. In a complimentary project, Headen and Hoepfner presented the limitations of current modeling approaches and recommended improvement strategies for predicting a subset of hypothetical asphaltene structures. 44 This previous study utilized the data discussed in this work to compare to calculated scattering results on the molecular scale and nanometer scale. The conclusion was that simulated structures failed to reproduce key features in the experimental measurements, including the spatial separation between aromatic-rich and -poor regions of asphaltene molecules due to the limited length/time scale that can be achieved by atomistic simulations. Specifically, the results demonstrated that either the common simulation approaches/forcefields are inaccurate, molecular representations of asphaltenes are incorrect, or the scale of simulations needs to be expanded to include more molecular polydispersity, a greater number of molecules, and a longer simulation duration. Previous atomistic simulations revealed that including greater molecular polydispersity improves the predictions of experimental asphaltene behavior. 45 Moreover, the molecular information from this work can validate molecular structures observed using non-contact Atomic Force Microscopy. 46,47

This study is designed to reveal the relationship between the molecular association of nano-aggregates and fractal clusters as a function of solid vs. liquid-dispersed asphaltenes, different level of stabilities from asphaltene subfractions, and temperature. Investigating the local structures of asphaltenes in mixtures of solvents at both the molecular and fractal cluster length scales using wide-angle neutron scattering or diffraction (WANS/ND) and small-angle neutron scattering (SANS) will reveal how ordering inside the nano-aggregates correlates to the self-assembly of clusters and

ultimately phase behavior. Furthermore, the results from this work provide the experimental data to serve as a benchmark for future molecular simulation of asphaltenes.

2. Experimental Methods

Asphaltene Sample Preparation. To explore the effect of asphaltene stability on assembly characteristics, two solid asphaltene samples were extracted from Athabasca bitumen, using pure heptane (H100) as the diluent and an 80 vol. % heptane with 20 vol. % toluene mixture (H80). The H80 asphaltene samples represent a sub-fraction of asphaltenes that are less stable as they are closer to their phase transition point and will precipitate with a lower quantity of heptane in the mixture. In this extraction, the H100 diluent was added to bitumen into a 40:1 by weight ratio while H80 was added to the oil at 20:1. The mixture was stirred for 24 hours and the solids were separated by centrifugation at 3472 g-force for 10 minutes. Solid asphaltenes were washed for 24 hours in a Soxhlet extractor with pure heptane to remove any maltenes trapped in the cake. The cake was then dried in a vacuum oven at 80 °C for four days to remove any residual heptane. An additional step was performed due to the presence of inorganic solids in Athabasca bitumen.⁴⁸ The solid asphaltene samples were diluted to a 4.8 wt. % solution in toluene and centrifuged at 5000 g-force for 270 minutes to separate inorganic solids. The toluene was then removed by forced convection and dried in a vacuum oven at 80 °C to obtain the solid asphaltene samples. No sharp crystalline peaks were observed in the wide-angle scattering, indicating that any remaining inorganic solids did not significantly contribute to the measured diffraction patterns. Liquid-dispersed samples were prepared by first weighing the asphaltene powder, adding deuterated 1-methylnaphthalene (d-1-MN) (d10, >98 % deuterated, Sigma-Aldrich), and stirring at 80 °C to form a homogeneous mixture at 25 wt. % asphaltenes. The solvent d-1-MN was selected due to its ability to disperse asphaltene samples in the liquid phase and its high boiling point (c.a. 244 °C) to facilitate elevated temperature experiments without significant pressurization of the sample holder.

Wide-Angle and Small-Angle Scattering Experiments. The Near and Intermediate Range Order Diffractometer (NIMROD) at the ISIS Pulsed Neutron and Muon Source⁴⁹ was used to assess neutron total scattering profiles (small- and wide-angle neutron scattering) on the Athabasca asphaltene samples. The momentum transfer range of the NIMROD instrument is approximately 0.02 Å-1 to 50 Å-1. The sample holders used with this instrument were flat plate "null-scattering" TiZr alloy cells with either a 1 mm (liquid samples) or 2 mm (solid powder samples) path length. Liquid samples where heated (approx. 80 °C) to reduce the viscosity and then loaded into the TiZr cells with a syringe. The cells were then mounted to an oil-bath controlled variable temperature sample holder. Additionally, the scattering of neat liquid d-1-MN was also measured at the same temperatures as the asphaltene samples for background subtraction. Nominally, the temperatures used in the discussion of the results are 20, 70, 130, and 180 °C, and the measured values at the sample were 20±2, 69±2, 128±2, and 177±2 °C. The scattering patterns for the solid and liquid-dispersed H100 asphaltenes were collected upon cooling to investigate any apparent hysteresis. Data collection time for the solid asphaltenes was at least 3 hours, for the liquid-dispersed asphaltenes was 2 hours, for cooling hysteresis experiments was 1 hour, and for d-1-MN solvent backgrounds was 1 hour. Sample data collection times were increased as the hydrogen concentration increased due to the high incoherent and low coherent scattering cross sections for light hydrogen.

All results were analyzed by the standard instrument procedures and corrected for beam transmission, parasitic scattering, sample transmission, and sample holder and instrument background. Results were normalized by the number of atoms in the system and presented on an absolute scattering cross-section with units of barns/steradian/atom. This normalization approach differs from the small-angle neutron and X-ray scattering analysis that is commonly performed on asphaltenes. In small-angle scattering, it is more common to normalize results to the volume of the sample, and the units

are typically presented as cm⁻¹ (i.e., cm²/cm³); however, the analysis approach and theory does not differ.⁵⁰ The self-scattering, ^{51,52} represented by the following equation: $\sum_{j=1,N} c_j \langle b_j \rangle$, where c_j is the atomic fraction and $\langle b_j \rangle$ is the average scattering length, was also eliminated from the data such that the scattering intensity tended to 0 as q increased. Due to an unknown void fraction of the powdered solid asphaltene samples, a scaling factor was introduced to ensure that the predicted total scattering length matched with theoretical predictions from elemental composition analysis that is provided in the Supporting Information. As will be demonstrated in the results, this approach generated scattering patterns that matched the intramolecular scattering of asphaltenes regardless of whether the results were analyzed as solids or in the dispersed state. Additional discussion of data correction procedures is included below.

Scattering Theory. Elastic scattering experiments measure the intensity of scattered radiation as a function of the scattering vector, ⁵⁰

$$q = \frac{4\pi \sin\theta}{\lambda} = \frac{2\pi}{d} \tag{1}$$

where θ is the scattering angle, λ is the wavelength of the radiation, and d is the correlation distance in real space. The scattering vector has units of reciprocal length (e.g., Å⁻¹) and large structural features are measured at small angles or low-q, hence the application of small-angle scattering to measure the structural properties of colloidal or macromolecular systems. Conversely, at wide angles or high-q, the molecular-scale structure can be probed as is commonly performed with X-ray and neutron diffraction. The approximate real-space length-scale associated with a particular scattering feature in a diffraction result corresponds to $d = 2\pi/q$. The experimental results presented in this paper span from conventional small-angle scattering (c.a. $0.02 < q < 0.5 \text{ Å}^{-1}$) length scales to the wide-angle regime (c.a. $q > 0.5 \text{ Å}^{-1}$).

Small-Angle Scattering Data Analysis. Conventionally, the scattering intensity in the small-angle regime is described by I(q) (units cm⁻¹) and is related to the volume, concentration, shape (form factor), and interparticle structural correlation (i.e., structure factor):⁵⁰

$$I(q) = \phi \Delta \rho^2 V_p P(q) S(q) \tag{2}$$

where I(q) is the scattering intensity, ϕ is the volume fraction of asphaltene particles asphaltenes, $\Delta \rho^2$ is the scattering contrast, V_p is the particle volume, P(q) is the form factor that contains shape and structure information of the particles, and S(q) is the structure factor that describes the correlation between particles. The scattering length density (SLD), ρ , represents the likelihood of a material to scatter x-rays/neutrons, and the SLD can be calculated using the mass density and elemental composition of the materials. The scattering contrast, $\Delta \rho^2$, is the square difference between the SLD of asphaltenes and the liquid surroundings. In this investigation, only shape-independent size analysis was performed on the small-angle regime. The scattering results in the small-angle regime were modeled using the shape-independent Guinier approximation:⁵³

$$I(q) = I_0 exp(\frac{-q^2 R_g^2}{3})$$
(3)

where R_g is the radius of gyration, and I_0 is the zero-angle scattering intensity. The size estimate obtained from the Guinier fit (i.e., R_g) should be regarded as an effective size due to the high concentration of asphaltenes present in the systems investigated. Structure factor effects cannot be neglected for asphaltene solutions at concentrations higher than approximately 2 vol. %.⁵⁴ The zero-angle scattering intensity for a dilute system is related to the total volume of scattering material, the molecular weight, or number density given a known mass density and volume fraction.²⁹ Again, due to the high concentration of the samples investigated, changes in the zero-angle scattering intensity

should be viewed as effective reductions in the total volume of the particles (or molecular weight) or a reduction of the impact of structure factor effects (e.g., reduced interparticle correlation).

Wide-Angle Scattering Data Analysis. The wide-angle scattering regime contains both intermolecular and intramolecular structural information. The intensity at higher scattering vectors, q, probe smaller structures, which is inversely proportional to the separation/correlation distance, d. In the wide-angle scattering results, intermolecular correlations between molecules are predominantly observed at lower q, while the intramolecular interactions are probed at higher q and describe correlation between atoms or moieties within a molecule.⁴²

In this study, atom-normalized results of the total structure factor, F(q), follow the convention of the wide-angle regime analysis (e.g., units of barns/steradian/atom). For an arbitrary system, experiments measure the total structure factor, F(q), that can be written as a weighted summation of individual contributions from partial structure factors, $S_{\alpha\beta}(q)$ describing the organization of two particle types (α and β):

$$F(q) = \sum_{\alpha,\beta>\alpha} (2 - \delta_{\alpha\beta}) c_{\alpha} c_{\beta} \langle b_{\alpha} \rangle \langle b_{\beta} \rangle (S_{\alpha\beta}(q) - 1)$$
(4)

where $\delta_{\alpha\beta}$ is the Kronecker delta (1 if $a=\beta$, 0 otherwise), c_{β} is the atomic fraction, is the average scattering length. A weighting factor substitution can be introduced to make the expression above more compact: $\omega_{\alpha\beta} = (2 - \delta_{\alpha\beta})c_{\alpha}c_{\beta}\langle b_{\alpha}\rangle\langle b_{\beta}\rangle$. The partial structure factor, $S_{\alpha\beta}(q)$, describes the spatial arrangement information of the atom types α and β in reciprocal space and can be calculated from a known configuration by a Fourier transform of a partial radial distribution function, $g_{\alpha\beta}(r)$:

$$S_{\alpha\beta}(q) = 1 + \frac{4\pi n}{q} \int_0^\infty r[g_{\alpha\beta}(r) - 1] \sin(qr) dr$$
(5)

for $q \neq 0$, where n = N/V is the atomic number density, and r is the real-space separation distance.

The systems studied in this project contain asphaltenes with vast molecular polydispersity and complexity; consequently, separating all possible correlations between atoms of different types from the diffraction data is infeasible. Therefore, the system was simplified to study the three broad structural correlations: asphaltene-asphaltene (A-A), asphaltene-solvent (A-S), and solvent-solvent (S-S). Following this approximation, Equation 4 can be rewritten as:

$$F(q)_{sample} = \omega_{AA}(S_{AA}(q) - 1) + \omega_{AS}(S_{AS}(q) - 1) + \omega_{SS}(S_{SS}(q) - 1)$$
(6)

The primary goal of this investigation was to assess the structure of the asphaltene-asphaltene organization, $S_{AA}(q)$. To extract this information from the total structure factor, two necessary simplifying assumptions were made: (1) the solvent-solvent structure factor, $S_{SS}(q)$, is unaffected by the presence of asphaltenes, and (2) there are no structural correlations between the asphaltenes and solvent (i.e., $S_{AS}(q) - 1 = 0$). In the absence of specific interactions between the solvent and asphaltenes, we see this approach as a reasonable assumption in order to obtain generalized information on the structure of asphaltenes in solution. Also, the highly associating structure of asphaltenes will reduce the total surface area of contact between asphaltenes and solvent, reducing the magnitude of $S_{AS}(q)-1$, and mitigating the impact of neglecting this contribution. The accuracy of these assumptions was not directly assessed and additional simulation investigations are recommended. However, due to the vast molecular complexity of asphaltenes, it may not be feasible to know whether differences in simulated structures and the analysis approximations presented in this study are due to unexpected consequences of the assumptions or inaccuracies in the simulations.

Using the stated approximations, the scattering associated with asphaltene structure can be extracted from manipulation of the mixed (asphaltenes plus solvent, i.e., "sample") and the solvent-only sample (i.e., "bkgd"). The scattering from solvent molecules alone was eliminated by subtracting

the solvent only total structure factor $F_{bkgd}(q)$ weighted by the atom fraction of solvent in the mixed sample (c_s), and normalized to the atom fraction of asphaltenes:

$$F(q) = \frac{1}{c_A} (F(q)_{samples} - c_s F(q)_{bkgd}) \tag{7}$$

where c_A is the asphaltene atomic fraction and c_S is the solvent atomic fraction ($c_A + c_S = 1$). Normalization by the asphaltene atom fraction is performed to compare the solvent-dispersed results directly to the solid-phase samples where $c_A = 1$.

Due to the light hydrogen content in asphaltenes, inelastic scattering contributes to the measured neutron diffraction patterns as a background and contains no structural information. 51,52,55,56 As the hydrogen in asphaltenes cannot be replaced with deuterium, the inelasticity effect in asphaltenes cannot be trivially mitigated. Unfortunately, the region in q-space most impacted by inelastic hydrogen scattering (approx. $q < 5 \text{ Å}^{-1}$) coincides with the length scales containing insight into the intermolecular structure. Consequently, it is crucial to eliminate the inelastic scattering from the data to obtain reliable structural information. The scattering results collected on NIMROD data were reduced using the Gudrun package with an iterative method of alternative binning the data in q-space for removing inelastic scattering effects. 57 For the liquid dispersed samples, small deviations in the background levels were noted after inelastic scattering subtraction and additional precautions were taken. This additional step to remove inelastic scattering contributions will be discussed in the Results section in greater detail. Additional details of this data analysis approach and a summary of all neutron total scattering results can be found in the Supporting Information.

3. Results

The results and discussion will first present the total scattering results and focus on the interpretations of the larger structures that are observable in the small-angle regime. Then the analysis

of the wide-angle results will highlight local molecular-scale structural changes that were observed. Finally, a comparison between the two length scales will be explored to discuss the molecular-scale driving forces that induce larger asphaltene associations.

Neutron Total Scattering Results. Figure 1 shows a general overview of the neutron total scattering data and a comparison of dispersed asphaltenes in the liquid phase and solid asphaltenes. The profile contains two regimes (approximately separated by blue dashed line): small-angle scattering $(0.02 < q < 0.5 \text{ Å}^{-1})$ and wide-angle diffraction $(q > 0.5 \text{ Å}^{-1})$. The two regimes were analyzed separately as described in the previous section. The results were also shifted by +1 for F(q) to avoid negative numbers on the log-log plot.

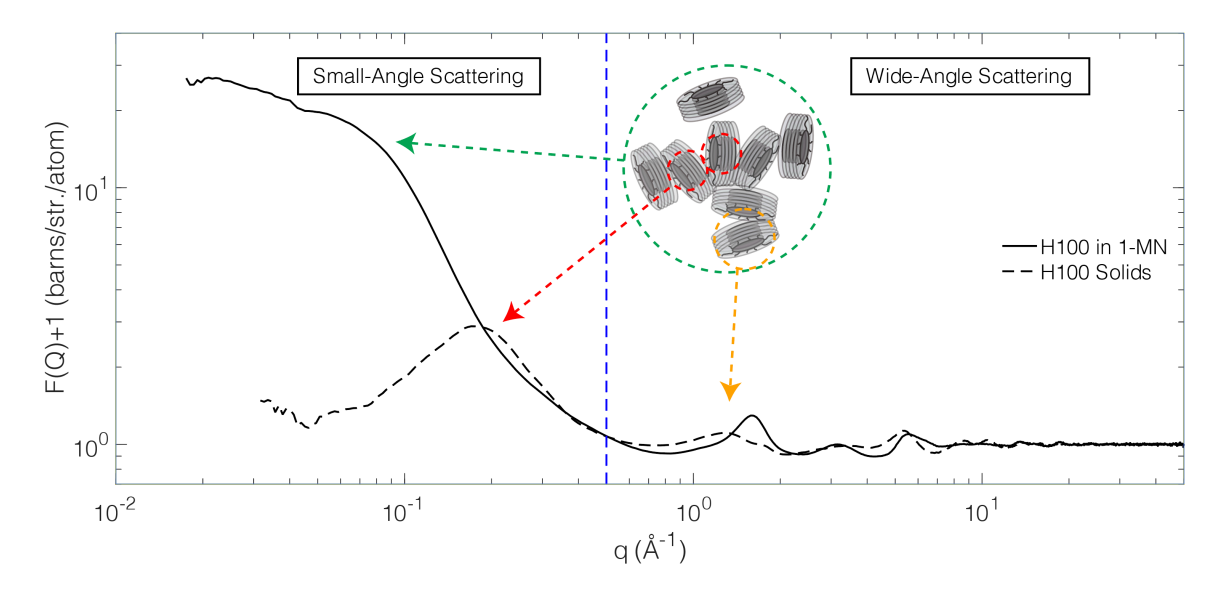


Figure 1: Neutron Total Scattering Data Overview: Small-Angle + Wide-Angle. Comparison of liquid dispersed and solid asphaltenes. Dashed line: solid H100 powder; Solid line: H100 dispersed in d-1-MN at 25 wt.% with the y-axis shifted by +1 to avoid negative numbers in the log-log plot. Blue dashed line approximately separates the small-angle and wide-angle scattering regions at $q = 0.05 \text{ Å}^{-1}$.

In Figure 1, the solution-dispersed sample shows a typical small-angle regime that can be used to assess the radius of gyration of asphaltenes using appropriate models (e.g., Guinier fit). In solids asphaltenes, the small-angle scattering region shows a peak at 0.18 Å⁻¹ that represents the structural

Å.44,58 We note that the only hysteresis observed in the experiments was found in a shift in this characteristic distance between aromatic regions in the solid phase samples. Upon heating, and preserved during cooling, the aromatic region separation distance shifted from approx. 35 Å to 39 Å and the peak breadth was also skewed to lower *q*-values, indicating that this length scale may correspond to a glassy state for asphaltenes. Increasing the temperature may encourage the aliphatic and aromatic regions of asphaltenes to further segregate. See Supporting Information for the results highlighting this shift.

The features in the WANS regime ($q > 0.5 \text{ Å}^{-1}$) correspond to the local intermolecular and intramolecular structure of the samples. Each peak approximately describes different structural correlations in asphaltenes and the solvents. Using reference compounds for comparison,² the peak positions can be used to infer different corresponding features (e.g., aromatic stacking). Peak heights (maximum intensity) and breadths represent the total quantity, size of the repeating structure, and polydispersity distribution/volume-averaged size of each structure in the system.^{2,8,28,51,52,59-42} Polydisperse or small sized repeating structures produce broad peaks, while well-defined repeating structures with long-range order (i.e., crystalline) produces sharp, narrow peaks. In this work, the discussions are focused on the intermolecular region (0.2 < $q < 2 \text{ Å}^{-1}$) to study the interactions between molecules. It was suspected that the intramolecular interactions at approximately $q > 7 \text{ Å}^{-1}$ would not be significantly modified by changes in temperature or concentration (at the range of temperature or dilution ratio studied in this paper).^{8,44} The intramolecular region was used to evaluate the performance of data correction procedures, and the profiles of solid vs. liquid dispersed asphaltenes in this range should align if the correction procedure is applicable. The correlation information at the intramolecular scale could also be used to provide molecular polydispersity information in

simulations⁴⁴ and to benchmark non-contact atomic force microscopy^{46,47} results on asphaltene chemical structure observations.

Small-Angle Scattering: Cluster and Nano-Aggregate Assembly. Figure 2 shows the small-angle scattering profiles of asphaltenes dispersed in d-1-MN for the two subfraction samples (H80 and H100) at the two extreme temperatures, 20 and 180 °C. At the small-angle length scale, shape-independent size analysis was performed using the Guinier approximation (shown in dashed lines) to assess structural information of the larger asphaltene assemblies.

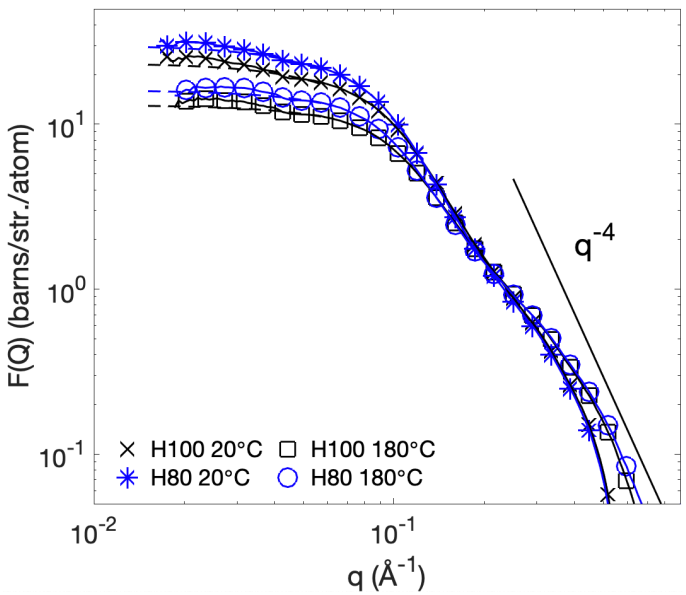


Figure 2: Small-angle scattering results with Guinier fits (dashed curves) for asphaltenes in d-1-MN at 25 wt. %. Solid line of q^4 indicates Porod surface scattering limit.

As discussed in the data analysis section, due to the high concentration of asphaltenes (25 wt. %), the structure factor, S(q), cannot be neglected in the small-angle scattering analysis procedure. Therefore, the size estimates obtained from the Guinier fit should be regarded as *effective* sizes. Figure 2 demonstrates that the H80 asphaltenes show a greater scattering intensity than H100, indicating a larger volume or greater quantity of large-scale clusters. The small-angle scattering results for the

dispersed samples at all temperatures were fit using the Guinier approximation, and the radius of gyration, R_2 , and zero-angle intensity, I_0 , from the fit are presented in Figure 3.

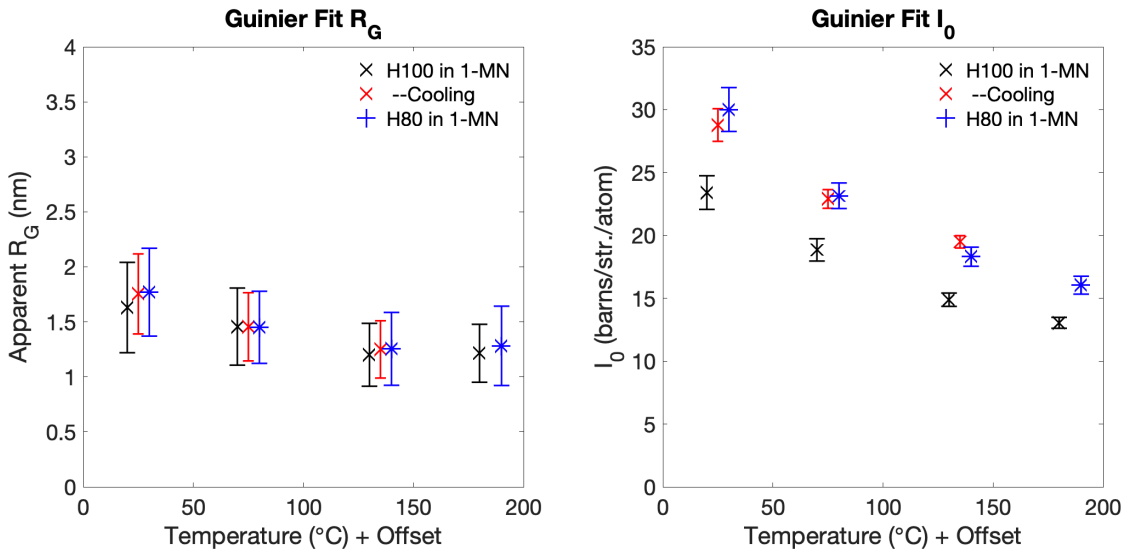


Figure 3: Effective radius of gyration R_g and zero-angle intensity I_θ as a function of temperature for both H80 and H100 samples dispersed in d-1-MN. Left figure: radius of gyration; Right figure: zero-angle intensity. Data collected on the H100 samples during cooling noted no apparent hysteresis in the results. Results for H100 samples upon cooling and H80 samples are offset by 5 °C and 10 °C, respectively for clarity.

The radius of gyration was measured to be largely unchanged as a function of asphaltene subfraction and showed a gradual reduction in size as a function of temperature, but relatively minor with respect to the uncertainty. This finding is in contrast to previous SANS work⁶³ where the radius of gyration for 5 wt. % asphaltenes in d-1-MN was observed to decrease from approximately 4.7 nm at 20°C to 1.2 nm at 400°C. The limited change in size observed in the current investigation is likely due to interparticle structure factor effects overwhelming actual size changes or there may be only a small decrease in cluster size due to the self-solubilization induced by the high (25 wt. %) asphaltene concentration. As the asphaltene concentration increases, the total solution environment will become more "asphaltene-like" and may result in a self-solubilization effect that aids in stabilizing asphaltene clusters at smaller size. This analysis is consistent with previous measurements of asphaltene cluster sizes that are significantly larger, around 2-8 nm when dispersed at concentrations <5 vol. %. ¹⁰ We

anticipate that increasing the asphaltene concentration will increase their stability (i.e., decrease association size) akin to the behavior of a polymer in a melt or when dispersed in a theta solvent. In these situations, the mixing excess free energy will tend toward zero, and the solution will behave as though it is pure and in an ideal mixing environment.⁶⁴ Unlike the size measurements, I_{θ} does exhibit a clear decrease at elevated temperatures, indicating a decrease in the total volume or quantity of larger structures. This observation likely arises from the dissociation of clusters and/or nano-aggregates as the temperature increases: clusters break into nanoaggregates and/or nano-aggregates dissociate into monomers (i.e., molecularly dispersed). A similar phenomenon was discovered in previous work that the dissociation of asphaltene nano-aggregates occurs during dilution from concentrations of 2 wt. % down to 15 mg/L in solution.¹⁰

Moreover, the dispersed H80 samples exhibit higher zero angle intensity, I_0 , compared to H100 along the entire temperature scale, indicating a greater quantity of assembled structures exist in the H80 sample regardless of the temperature. This structural difference between H100 and H80 at the larger length scales aligns with previous studies regarding the degree of association increasing with decreasing asphaltene stability. 12,65-67 As introduced in the sample preparation section, H80 powders were extracted by adding a lower quantity of heptane into bitumen compared to H100, consequently the H80 asphaltenes are expected to be more unstable and nearer to their phase transition point from solution. Previous small-angle scattering analysis has revealed that asphaltene clusters increase in size as they approach their phase transition, and the measurements here further support this conclusion. 10

Wide-Angle Scattering: Local Molecular Ordering. The mechanism of asphaltene self-assembly into larger structures observed in the small-angle region was related to structural correlations at the molecular scale using wide-angle scattering results. Figure 4a presents the wide-angle regime

results for H100 and H80 samples in the solid phase and dispersed in d-1-MN. Figure 4b demonstrates the effect of the solvent background elimination and normalization by the asphaltene atom fraction.

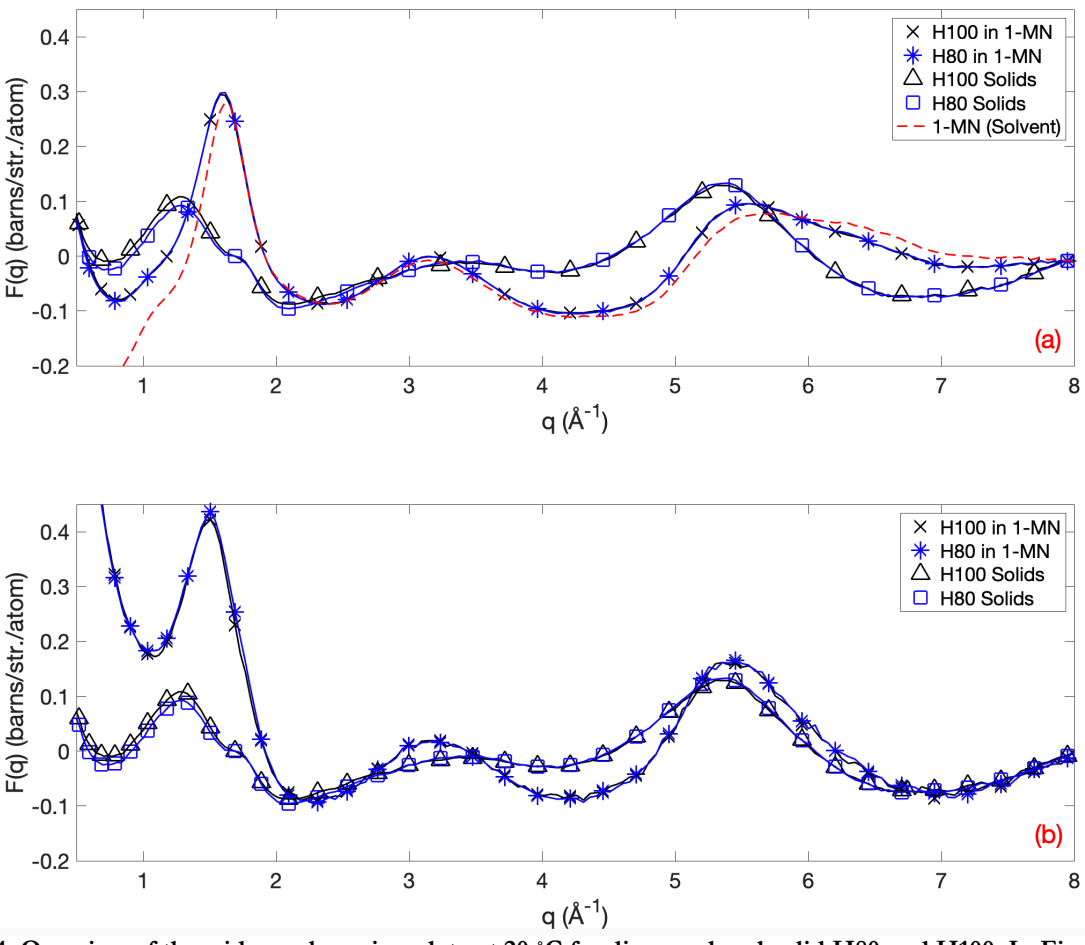


Figure 4: Overview of the wide-angle regime data at 20 °C for dispersed and solid H80 and H100. In Figure (a), the scattering patterns of dispersed samples were not corrected with the solvent d-1-MN background. Figure (b) shows the profiles after the solvent background subtraction and normalization with the asphaltene atom fraction.

The solid asphaltene scattering profiles in Figure 4 are similar to previous X-ray diffraction results.^{2,3} The peak at approx. 1.3 Å⁻¹ has been previously interpreted as alkyl side chain interactions, typically called the γ peak; however, in this report we refer to this peak as the "disordered peak" as to not ascribe a particular type of organizational feature (e.g., hydrogen-bonding/supramolecular network,⁶⁸ naphthenic interactions⁶⁹). The peak at approx. 1.8 Å⁻¹ is better defined due to its similar position to the [002] graphite spacing and represents the stacking of aromatic areas in asphaltene nanoaggregates.² For dispersed samples in d-1-MN, Figure 4a shows the results before the d-1-MN

background elimination. The solution-dispersed datasets show a similar pattern compared to the pure solvent before solvent background subtraction, indicating the dispersed asphaltene signals are hidden by the peak at 1.6 Å⁻¹ for d-1-MN. The scattering from the 75 wt. % solvent was then removed to isolate the scattering contribution of the dispersed-phase asphaltenes (Figure 4b). Figure 4b includes scattering signals after the solvent correction, which predominantly presents the contributions by asphaltenes. For q > 7 Å⁻¹, we see the solvated and solid phase asphaltene scattering results superimpose, indicating that the normalization procedure is appropriate for comparing the samples as a result of the intra-molecular structure being similar between the samples.

The steady scattering intensity increase for $q < 2 \text{ Å}^{-1}$ is interpreted as an artifact from the incomplete removal of the inelastic scattering during data processing, or as a result of small-angle scattering artifacts persisting to higher q-values. As discussed in the Methods section, uncertainties from the inelastic scattering corrections persisted and were amplified when isolating the asphaltene scattering contribution. Previous work has demonstrated that the shape of the inelastic effect in neutron scattering to be monotonically decreasing with increasing q and contribute to the distinct elevation of I(q) at a lower q values. 50,55,56,70 This observation reveals that for a narrow region in q-space, the inelastic scattering contribution will not have any sharp features or sudden changes in intensity. Consequently, a linear background subtraction to the inelastic scattering was implemented to both the dispersed and solid phase samples to provide for consistent quantitative comparisons. The procedure of this empirical linear correction and additional details are presented in the Supporting Information.

Figures 5a-d present the results after the inelastic scattering correction procedure for the regime between approx. 0.5 and 2 Å⁻¹ as a function of temperature for the solid and dispersed phase samples. As shown in Figures 5a and c, solid asphaltenes demonstrate two clear peaks, the disordered peak, at approx. 1.25 Å⁻¹ and the [002] graphitic peak, at approx. 1.7 Å⁻¹. For the liquid dispersed samples in Figures 5b and d, asphaltenes have a more prominent single peak (c.a. 1.5 Å⁻¹), but a knee

in the results can still be identified at approx. 1.7 Å⁻¹. The clearly distinguishable peaks for the disordered and [002] structures in solid asphaltenes reveals local separation of the aliphatic and aromatic regions, presumably due to their compositional difference. However, when dispersed in solution, the disordered peak increases in amplitude and shifts to nearer separation distances (i.e., higher q). This observation reveals a substantial change in local conformation of asphaltenes upon dissolution and highlights the significance of the solution environment on asphaltene local structure. Future simulation comparisons with the experimental results may shed light on the nature of this change in structure upon dissolution. Additional discussion of these trends and a comparison of the asphaltene sub-fractions (H100 and H80) is provided below following quantitative analysis of the peak amplitudes and positions.

Quantitative assessment of the changes in peak position and intensity in the scattering profiles was obtained by fitting the wide-angle scattering results with two Gaussian functions for the disordered and [002] peaks. Representative examples of the fit quality are shown in Figures 5e and f. From the Gaussian fits, the positions and intensities of the disordered and [002] peaks could be obtained. Additionally, Figure 6 presents the peak amplitudes and positions in real space from the analysis of the Gaussian fits obtained by analyzing the results in Figure 5. Details on the fitting and uncertainty estimation procedure are included in the Supporting Information.

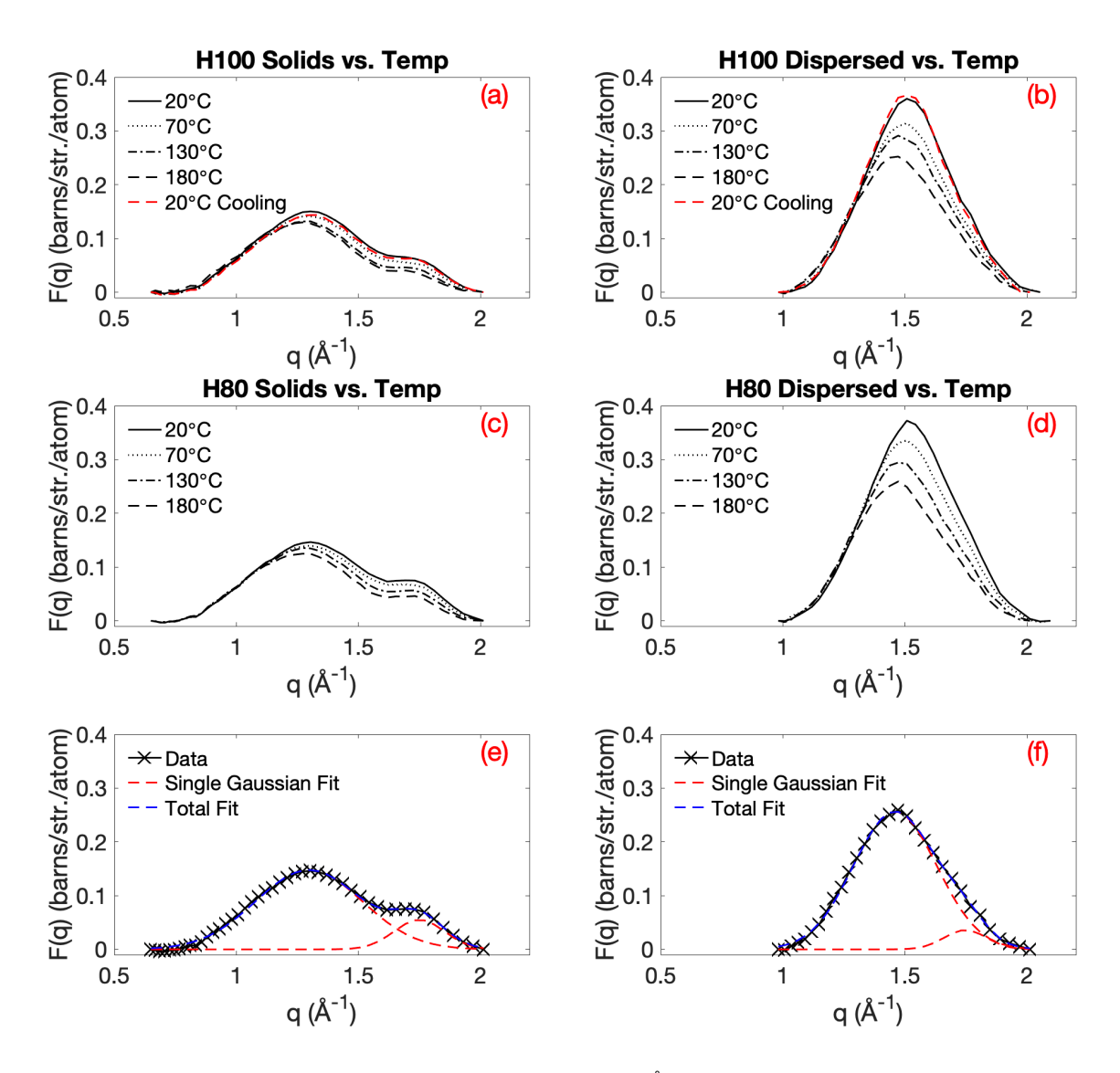


Figure 5: Profile of wide-angle scattering peaks from $0.5 < q < 2 \text{ Å}^{-1}$ and representative Gaussian fits. (a-b) Solid and dispersed H100 asphaltenes vs. temperature. (c-d) Solid and dispersed H80 asphaltenes vs. temperature. H80 asphaltenes show a more pominant [002] peak at approx. 1.7 Å⁻¹ compared to H100 samples. (e) Representative Gaussian curve fit for solid H80 asphaltenes at 20 °C. (f) Representative Gaussian curve fit for dispersed H80 asphaltenes at 180 °C.

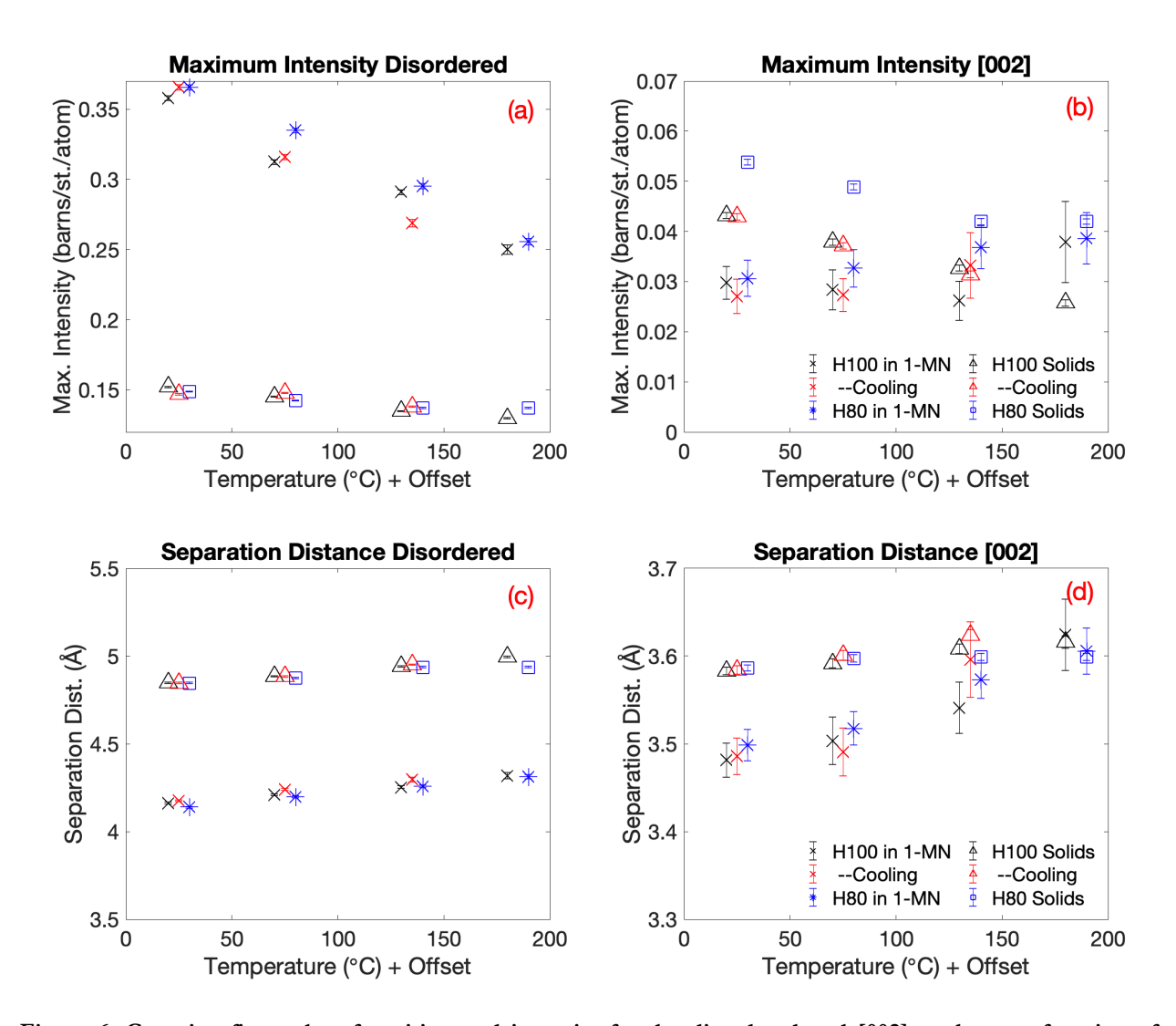


Figure 6: Gaussian fit results of position and intensity for the disordered and [002] peaks as a function of temperature and sample. (a) disordered peak maximum intensity (b) [002] peak maximum intensity (c) disordered peak separation distance (d) [002] peak separation distance. Measurements upon cooling were probed for the H100 samples in both the solid and dispersed phase and show no apparent hysteresis. Results for H100 samples upon cooling and H80 samples are offset by 5 °C and 10 °C, respectively for clarity.

The results in Figure 5 demonstrate that the Gaussian fits of the peak profiles produce an excellent representation of the scattering results in the wide-angle regime to assess the intensities and positions of the various intermolecular structures present in both solid and dispersed-phase asphaltenes. Several trends are clear in the results, with many following expectations, whereas others were counterintuitive. No apparent hysteresis was observed for the wide-angle scattering results and the conclusions can largely be assessed as thermodynamic in origin. For the intuitive and expected

observations, all samples and structural features exhibited a shift to larger length scales as the temperature increases, and this behavior is attributed to thermal expansion (Figures 6c-d). Additionally, the intensity or extent of the structural correlations reduced (Figures 6a-b) as the temperature increased, save for the [002] peak in the dispersed phase systems where an increase in order was observed. This increase is gradual for the H100 sample and most identifiable at the highest temperature, but the trend is apparent with the dispersed H80 asphaltenes. As the temperature is increased, the system is expected to tend toward more disorder (i.e., reduced scattering peak amplitudes) due to the thermal energy of the system (i.e., k_bT) increasing and becoming more significant relative to any intermolecular potential energy stored in various structural features. The disordered peak amplitude in the solid samples reduces at a similar rate as the [002] peak amplitude; however, this effect is difficult to visualize in the plots above due the difference in the y-axis scaling of Figure 6a. The total amplitude of disordered peak is significantly larger when dispersed in d-1-MD, and this observation generally supports the hypothesis that there are more abundant disordered interactions than planar stacking shown in the [002] peak; however, we cannot rule out the impact of solvent-asphaltene structural correlations having an impact. If a specific interaction between the solvent and asphaltenes occurs at a similar length scale as the measured disordered peak in asphaltenes, there may be artifacts of neglecting this association when performing the solvent background subtraction as performed in this investigation. Absent impact from solvent-asphaltene correlations at this length scale, the results indicate that asphaltene side-chain interactions represent the dominant mechanism for association when dispersed. Minimally, the findings highlight that [002] stacking is not the sole form of interaction between asphaltenes or nano-aggregates. This finding is in agreement with solid-state NMR measurements of asphaltenes that also suggest significant influence from side-chain interactions from asphaltenes.³⁵ These observations will be further expanded on when comparing

between the larger length scale interactions probed in the small-angle scattering regime to that of the local molecular spacings discussed in this section.

The presence of a solvent when analyzing the dispersed phase samples introduces important additional considerations, specifically, entropic contributions to order as a result of solvent depletion interactions. 71,72 Isothermal systems obtain their equilibrium state when free energy is minimized (G =H-TS), which contains contributions from both energy and entropy. Increases in structure as the temperature increases can be often attributed to entropic driving forces for assembly.⁷³ Consequently, the observations that dispersed asphaltenes actually increase in order for the [002] stacking peak is thermodynamically-consistent with an entropic driving force for assembly. The mechanism for such an observation is consistent with the solvent d-1-MN forcing asphaltene molecules into a state of greater order such that the mixture increases the overall accessible free volume. This mechanism is also consistent with the reduction in the disordered and [002] peak separation distances of asphaltenes when comparing the solid and dispersed phase. When asphaltenes are dispersed in a liquid, the disordered peak and the [002] peak distances are decreased by approximately 0.6 and 0.1 Å, respectively, highlighting a closer packing that may be induced by solvent depletion forces. Additionally, the separation distance for the [002] peak in the dispersed and solid phase samples converge around a similar point at 180 °C. These observations support the overall analysis approach and demonstrates a consistent measurement of the local asphaltene structure between the solid and dispersed phase state.

While entropy may induce structure in dense fluid mixtures (e.g., liquids), there is a temperature limit to which the extent of free volume effects will induce structure versus the competing driving force for kinetic or thermal effects to push the fluid towards a more ideal gas or unstructured state. It is also interesting to note that the H100 sample demonstrates a lower rate of increase (or limited change) in the [002] stacking as a function of temperature, and the highest value for the [002]

peak intensity at 180 °C demonstrates relatively significant uncertainty. In contrast the H80 sample shows a steady rate of increase with temperature, suggesting that the H80 asphaltenes are more susceptible to entropic forces of assembly, and this observation may shed light into why this subfraction is less stable. We can utilize the 180 °C (or approx. 450 K) temperature to estimate a back of the envelope lower bound for the entropic contribution to asphaltene association. At 450 K, the average kinetic or thermal energy (k_bT or RT) is 3.7 kJ/mol. Noting that previous estimates of the free energy of association (ΔG) for asphaltenes is on the order of -30 kJ/mol at 25 °C¹⁰, this estimate suggests that >10% of the association energy in solution may be entropic in origin. However, establishing a more accurate estimate that would account for both the enthalpic and entropic contributions to free energy over the studied temperature range would require more detailed thermodynamic modeling and is reserved for future study. We also note that temperature-dependent measurements of the DC-conductivity of asphaltenes also reveal a relatively robust nanoaggregate structure that does not readily dissociate at elevated temperature, further supporting the significant contribution of entropy to asphaltene association.⁷⁴

The impact of entropic solvent forces on asphaltene behavior is currently an underexplored area and may shed light into the complex process of asphaltene behavior in mixed solvents. Thermodynamically, certain liquid mixtures exhibit positive excess entropy of mixing that may at first seem counterintuitive. Positive excess entropy of mixing corresponds to a mixed solution where the total entropy is larger than expected based on simple ideal gas or random mixing. These systems rather exhibit a structured mixing process that produces a greater total entropy. Mixtures of weakly interacting compounds, like hydrocarbons, are classes of materials that generally exhibit positive excess entropy of mixing, and the impact of entropic effects on asphaltene assembly may be a valuable future research avenue. Indeed, the toluene-heptane mixture is such an example of a mixing

process that exhibits positive excess entropy of mixing⁷⁶ and is prolific in the investigation of asphaltene behavior.

One final comparison that can be made in the wide-angle scattering results are the differences between the H80 (less stable) and H100 asphaltene samples. In the solid phase, no apparent differences are observed for all experiments as a function of temperature, save for an approximately 25% increase in the scattering intensity for the [002] stacking at 20°C. As the rate of decrease in the [002] scattering amplitude is similar between the H80 and H100 asphaltene samples, this observation reveals that there is a subset of asphaltene molecules that are strongly bound in the [002] stacking orientation that are largely unaffected by the temperature increase. Consequently, the asphaltenes that are present in the H80 sample exhibit a higher preference for [002] stacking that is more energetically favorable compared to the remaining asphaltenes. Previous research also demonstrated similar observations when investigating the X-ray diffraction of asphaltenes separated by solubility where less stable asphaltenes were found to have a greater extent of aromatic stacking. However, as will be discussed in the following section, this observation does correlate with the asphaltene instability but it may not be the dominant cause of this behavior.

Correlation between Small-Angle and Wide-Angle Regimes. We conclude our analysis of the neutron total scattering results of asphaltenes by correlating the behavior of large-scale association of asphaltenes on the nanometer length scale with the local molecular structural changes. As the temperature was increased, the zero-angle scattering intensity, I_0 , decreased. However, on the local molecular scale, the [002] stacking increased and produces an opposite correlation with the large assembly characteristics. Consequently, Figure 7 presents a normalized correlation relative to the scattering amplitudes of I_0 and the disordered stacking of the asphaltenes with the reference scattering amplitudes representing the greatest amplitude that was observed at 20 °C.

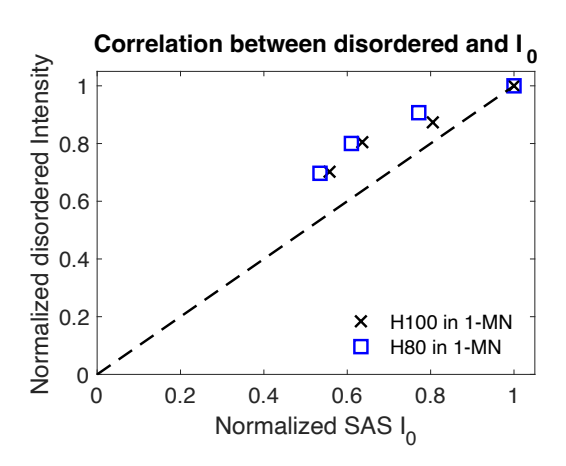


Figure 7: Small-angle and diffraction region correlation between the normalized scattering intensities of the I_{θ} and disordered peak in the dispersed samples. Uncertainty in the parameters is smaller than the marker size and not shown.

As shown in Figure 7, the local molecular disordered peak amplitude reduction is generally proportional to the observed decrease in scattering intensity of the large-scale associations. This finding suggests that the behavior of asphaltenes as a function of temperature is dominated by the interactions between asphaltene side-chains for temperatures <180 °C. One observation that is not yet resolved is the role of the [002] stacking in the large-scale cluster formation. We observed that the H80 asphaltene samples that are less stable form a greater number of nanometer sized clusters also exhibit greater [002] aromatic stacking. However, as the [002] stacking was observed to increase with respect to temperature, the overall dissociation of clusters on the nanometer length scale cannot be attributed to changes in the planar stacking. One mechanism that is consistent with the experimental observations is that the increase in [002] stacking for the H80 samples produces a larger sized nanoaggregate. If the asphaltene molecules assemble into a coin stack-like shape, the increase in [002] stacking will create a cylinder with both a larger height and also a greater surface area along the radial direction. The additional asphaltene molecule(s) will not increase the number of aromatic-aromatic interactions between asphaltene nanoaggregates as the total cross-sectional area of the aromatic region

will be unchanged. However, the surface area on the radial edge of the cylinder will increase and produce more locations for side-chain interactions. Consequently, while the greater extent of [002] stacking correlates to asphaltene instability, the aromatic-aromatic interactions between asphaltene nano-aggregates may not be the dominant driving force for observed instabilities. Rather, the increase in the [002] may produce larger nano-aggregates that have a greater surface area for disordered interactions.

The wide-range of scattering vectors explored in this study have provided novel insight into the correlations between local molecular organization and large-scale asphaltene clustering that has been previously shown to serve as a useful predictor of stability. 11 Consequently, in this work and a complimentary simulation study,⁴⁴ we present a road map of how to bridge detailed molecular-scale characterization techniques^{47,77} to bulk phase and fouling behavior using the local self-assembled structure as a link between these length scales. However, the analysis presented here relies on a few simplifying approximations that were necessary based on asphaltene complexity, but that differ when investigating simplified fluids in a more rigorous manner. 43,78,79 We specifically note that there may be uncertainty introduced when neglecting the asphaltene-solvent correlations when probing the structure of dispersed asphaltenes. Any specific correlations between the solvent and asphaltenes have been assumed to be solely from asphaltenes due to neglecting this cross-correlation. However, one strength of the experimental measurements is the availability of a direct comparison to atomistic simulations. We include tabulated experimental results for all experiments as Supporting Information for future analysis by simulation techniques. Further, the solvent background subtraction and any additional assumptions in the experimental analysis can be replicated with simulation results to assess uncertainties and to validate molecular structures or simulation methodologies. For example, the assumption of no asphaltene-solvent correlations is readily assessed by computer simulation as asphaltene-asphaltene, asphaltene-solvent, and solvent-solvent contributions to the form factor can

be independently calculated to probe the analysis assumptions and investigate the impact of various solvents on asphaltene structure.

4. Conclusions

While much is still left to learn on the mechanisms of asphaltene self-association and phase behavior, we demonstrate that neutron total scattering can provide valuable insight into translating molecular properties of asphaltenes to collective assembly characteristics and phase behavior. Specifically, the measured diffraction patterns can serve as a valuable aid to benchmark atomistic modeling studies of asphaltenes as a one-to-one comparison between simulation predictions and experimental measurements at this length scale can be obtained. 44 Further, the wide range of scattering vectors explored in this study bridge the gap between the molecular to the self-assembled scale of asphaltene nanoaggregates and clusters. Small-angle and ultra-small-angle scattering experiments 11,80 have demonstrated that the size of the asphaltene cluster associations can be used to understand their bulk phase stability and precipitation mechanisms. However, understanding how differing molecular properties of asphaltenes, and the impact of the solvent environment and polydispersity, contribute to the formation of large clusters still remains unsettled. Were such a connection to be formed, the detailed molecular characterization obtained from high-resolution mass spectrometry77 and AFM/STM⁴⁷ could be combined with self-assembly approaches to unite molecular scalecharacterization with phase behavior and flow assurance predictions. The impact of the solvent environment on the molecular thermodynamics of asphaltene mixtures was further complicated with the observation that some assembly characteristics of asphaltenes may be entropic in origin and encourages further study. The extent of aromatic [002] stacking of asphaltenes was found to increase when they were heated in a dispersed phase state, which is consistent with an entropically-promoted assembly process. The proposed mechanism is that through ensemble behavior, the surrounding

solvent encourages asphaltenes to associate in order to produce more free volume for the surrounding liquid. Consequently, as the temperature is increased, local order is promoted in asphaltenes to increase the free volume for the solvent molecules to increase their entropy. Entropic solvent effects on asphaltene behavior have seem limited investigation and may represent a non-trivial contribution to overall asphaltene behavior. Additionally, correlations between asphaltene subfraction, molecular ordering, and nano-scale assembly, reveal that [002] stacking may not be the dominant contribution to asphaltene association on the nanometer length scale. Rather, we observed that the breakup of larger asphaltene clusters correlated to the dissociation of disordered side-chain interactions for asphaltenes. Asphaltenes that are more unstable do indeed exhibit greater [002] stacking; however, this increase may not be the sole cause of their decreased stability and larger cluster sizes in solvent mixtures. Increasing the number of aromatic stacks in an asphaltene nano-aggregate may produce more disordered interactions, and these types of associations may be significantly influencing asphaltene association and phase behavior.

Supporting Information

Elemental (CHNOS) analysis of solid asphaltene samples, neutron total diffraction patterns and tabulated experimental results, inelastic background subtraction procedure, and the Gaussian fitting procedure.

Acknowledgements

The authors thank the U.S. National Science Foundation (Grant CBET-1821762) and U.K. Engineering and Physical Sciences Research Council (Grant EP/R013195/1) for financial support. Additional financial support was also provided by ExxonMobil. Experiments at the ISIS Neutron and Muon Source were supported by a beamtime allocation RB1710282 from the Science and Technology

Facilities Council. Experimental scattering results are freely accessible at: https://data.isis.stfc.ac.uk/doi/study/103199840.81

References

- 1. Abraham, H. Asphalts and Allied Substances. (D. Van Nostrand Company, 1920).
- 2. Yen, T. F., Erdman, J. G. & Pollack, S. S. Investigation of the Structure of Petroleum Asphaltenes by X-Ray Diffraction. *Anal. Chem.* **33**, 1587–1594 (1961).
- 3. Mullins, O. C. et al. Advances in Asphaltene Science and the Yen Mullins Model. (2012).
- G. Ali Mansoori. Modeling of asphaltene and other heavy orgnic depositions. J. Pet. Sci. Eng.
 17, 101–111 (1997).
- 5. Pernyeszi, T., Patzkó, Á., Berkesi, O. & Dékány, I. Asphaltene adsorption on clays and crude oil reservoir rocks. *Colloids Surfaces A Physicochem. Eng. Asp.* **137**, 373–384 (1998).
- 6. Hirschberg, a., DeJong, L. N. J., Schipper, B. a. & Meijer, J. G. Influence of Temperature and Pressure on Asphaltene Flocculation. *Soc. Pet. Eng. J.* **24**, 283–293 (1984).
- 7. Rao, F. & Liu, Q. Froth treatment in athabasca oil sands bitumen recovery process: A review. Energy and Fuels 27, 7199–7207 (2013).
- 8. Andersen, S. I., Jensen, J. O. & Speight, J. G. X-ray Diffraction of Subfractions of Petroleum Asphaltenes. *Energy & Fuels* **19**, 2371–2377 (2005).
- 9. Fenistein, D., Barré, L., Broseta, D., Espinat, D., Livet, A., Roux, J.-N. & Scarsella, M. Viscosimetric and Neutron Scattering Study of Asphaltene Aggregates in Mixed Toluene/Heptane Solvents. *Langmuir* 14, 1013–1020 (1998).
- Hoepfner, M. P. & Fogler, H. S. Multiscale Scattering Investigations of Asphaltene Cluster Breakup, Nanoaggregate Dissociation, and Molecular Ordering. *Langmuir* 29, 15423–15432 (2013).

- 11. Hoepfner, M. P., Vilas Bôas Fávero, C., Haji-Akbari, N. & Fogler, H. S. The Fractal Aggregation of Asphaltenes. *Langmuir* **29**, 8799–8808 (2013).
- 12. Spiecker, P. M., Gawrys, K. L. & Kilpatrick, P. K. Aggregation and solubility behavior of asphaltenes and their subfractions. *J. Colloid Interface Sci.* **267**, 178–193 (2003).
- 13. Eyssautier, J., Levitz, P., Espinat, D., Jestin, J., Gummel, J., Grillo, I. & Barré, L. Insight into asphaltene nanoaggregate structure Inferred by small angle neutron and X-ray scattering. *J. Phys. Chem. B* **115**, 6827–6837 (2011).
- 14. Tanaka, R., Hunt, J. E., Winans, R. E., Thiyagarajan, P., Sato, S. & Takanohashi, T. Aggregates Structure Analysis of Petroleum Asphaltenes with Small-Angle Neutron Scattering. *Energy & Fuels* 17, 127–134 (2003).
- 15. Maqbool, T., Raha, S., Hoepfner, M. P. & Fogler, H. S. Modeling the Aggregation of Asphaltene Nanoaggregates in Crude Oil-Precipitant Systems. *Energy & Fuels* **25**, 1585–1596 (2011).
- Ting, P. D., Hirasaki, G. J. & Chapman, W. G. Modeling of Asphaltene Phase Behavior with the SAFT Equation of State. *Pet. Sci. Technol.* 21, 647–661 (2003).
- 17. Creek, J. L. Freedom of Action in the State of Asphaltenes: Escape from Conventional Wisdom. *Energy & Fuels* **19**, 1212—1224 (2005).
- Kraiwattanawong, K., Fogler, H. S., Gharfeh, S. G., Singh, P., Thomason, W. H. & Chavadej,
 S. Thermodynamic Solubility Models to Predict Asphaltene Instability in Live Crude Oils†.
 Energy & Fuels 21, 1248–1255 (2007).
- 19. Cimino, R., Correra, S., Bianco, A. D. & Lockhart, T. P. Solubility and phase behavior of asphaltene in hydrocarbon media. in *Asphaltene: Fundamentals and Applications* 97–130 (1995).
- 20. Hoepfner, M. P., Limsakoune, V., Chuenmeechao, V., Maqbool, T. & Fogler, H. S. A Fundamental Study of Asphaltene Deposition. *Energy & Fuels* **27**, 725–735 (2013).

- 21. Chaisoontornyotin, W., Haji-Akbari, N., Fogler, H. S. & Hoepfner, M. P. Combined Asphaltene Aggregation and Deposition Investigation. *Energy & Fuels* **30**, 1979–1986 (2016).
- 22. Chaisoontornyotin, W., Bingham, A. W. & Hoepfner, M. P. Reversibility of Asphaltene Precipitation Using Temperature-Induced Aggregation. *Energy and Fuels* **31**, 3392–3398 (2017).
- 23. Speight, J. G. The Chemistry and Technology of Petroleum, Fourth Edition. (CRC Press, 2006).
- Cimino, R., Correra, S., Sacomani, P. A. & Carniani, C. Thermodynamic Modelling for Prediction of Asphaltene Deposition in Live Oils. in SPE International Symposium on Oilfield Chemistry 14–17 (1995). doi:10.2118/28993-MS.
- 25. Mckenna, A. M. Detailed Characterization of Heavy Crude Oils and Asphaltenes by Ultrahigh Resolution Fourier Transform Ion Cyclotron Resonance Mass Spectrometry. PhD Dissertation, Florida State University, Department of Chemistry and Biochemistry (2009).
- 26. Chacón-Patiño, M. L., Rowland, S. M. & Rodgers, R. P. Advances in Asphaltene Petroleomics.
 Part 2: Selective Separation Method That Reveals Fractions Enriched in Island and Archipelago
 Structural Motifs by Mass Spectrometry. Energy and Fuels 32, 314–328 (2018).
- 27. Maqbool, T., Srikiratiwong, P. & Fogler, H. S. Effect of Temperature on the Precipitation Kinetics of Asphaltenes. *Energy & Fuels* **25**, 694–700 (2011).
- 28. Tanaka, R., Sato, E., Hunt, J. E., Winans, R. E., Sato, S. & Takanohashi, T. Characterization of Asphaltene Aggregates Using X-ray Diffraction and Small-Angle X-ray Scattering. *Energy & Fuels* 18, 1118–1125 (2004).
- Yang, Y., Chaisoontornyotin, W. & Hoepfner, M. P. Structure of Asphaltenes during Precipitation Investigated by Ultra-Small-Angle X-ray Scattering. *Langmuir* 34, 10371–10380 (2018).
- 30. Headen, T. F., Boek, E. S., Stellbrink, J. & Scheven, U. M. Small Angle Neutron Scattering (SANS and V-SANS) Study of Asphaltene Aggregates in Crude Oil. *Langmuir* **25**, 422–428

(2009).

- Ismail, M., Yang, Y., Chaisoontornyotin, W., Ovalles, C., Rogel, E., Moir, M. E. & Hoepfner,
 M. P. Effect of Chemical Inhibitors on Asphaltene Precipitation and Morphology Using Ultra-Small-Angle X-ray Scattering. *Energy and Fuels* 33, 3681–3693 (2019).
- 32. Durand, E., Clemancey, M., Lancelin, J.-M., Verstraete, J., Espinat, D. & Quoineaud, A.-A. Aggregation States of Asphaltenes: Evidence of Two Chemical Behaviors by 1H Diffusion-Ordered Spectroscopy Nuclear Magnetic Resonance. *J. Phys. Chem. C* 113, 16266–16276 (2009).
- Da Silva Oliveira, E. C., Neto, Á. C., Júnior, V. L., De Castro, E. V. R. & De Menezes, S. M.
 C. Study of Brazilian asphaltene aggregation by Nuclear Magnetic Resonance spectroscopy.
 Fuel 117, 146–151 (2014).
- Chinelatto Júnior, L. S., Cabral De Menezes, S. M., Honorato, H. D. A., De Oliveira, M. C. K.
 & Marques, L. C. D. C. Diffusion-Ordered Spectroscopy Nuclear Magnetic Resonance as an Alternative Technique to Improve Asphaltene Characterization. *Energy and Fuels* 32, 2793–2800 (2018).
- 35. Dutta Majumdar, R., Gerken, M. & Hazendonk, P. Solid-state 1H and 13C nuclear magnetic resonance spectroscopy of athabasca oil sands asphaltenes: Evidence for interlocking π-stacked nanoaggregates with intercalated alkyl side chains. *Energy and Fuels* **29**, 2790–2800 (2015).
- 36. Eyssautier, J., Espinat, D., Gummel, J., Levitz, P., Becerra, M., Shaw, J. & Barré, L. Mesoscale Organization in a Physically Separated Vacuum Residue: Comparison to Asphaltenes in a Simple Solvent. *Energy & Fuels* **26**, 2680–2687 (2012).
- 37. Glotzer, S. C. & Solomon, M. J. Anisotropy of building blocks and their assembly into complex structures. *Nat. Mater.* **6**, 557–562 (2007).
- 38. Soper, A. K. The radial distribution functions of water and ice from 220 to 673 K and at pressures up to 400 MPa. *Chem. Phys.* **258**, 121–137 (2000).

- 39. Soper, A. K. & Ricci, M. A. Structures of high-density and low-density water. *Phys. Rev. Lett.* 84, 2881–2884 (2000).
- 40. Luzar, A. & Chandler, D. Structure and hydrogen bond dynamics of water–dimethyl sulfoxide mixtures by computer simulations. *J. Chem. Phys.* **98**, 8160 (1993).
- 41. Soper, A. K. & Luzar, A. A neutron diffraction study of dimethyl sulphoxide—water mixtures. *J. Chem. Phys.* **97**, 1320–1331 (1992).
- Headen, T. F., Howard, C. A., Skipper, N. T., Wilkinson, M. A., Bowron, D. T. & Soper, A. K.
 Structure of π-π Interactions in aromatic liquids. J. Am. Chem. Soc. 132, 5735–5742 (2010).
- 43. F. Headen, T., L. Cullen, P., Patel, R., Taylor, A. & T. Skipper, N. The structures of liquid pyridine and naphthalene: the effects of heteroatoms and core size on aromatic interactions. *Phys. Chem. Chem. Phys.* **20**, 2704–2715 (2018).
- 44. Headen, T. F. & Hoepfner, M. P. Predicting Asphaltene Aggregate Structure from Molecular Dynamics Simulation: Comparison to Neutron Total Scattering Data. *Energy and Fuels* 33, 3787–3795 (2019).
- 45. Javanbakht, G., Sedghi, M., Welch, W. R. W., Goual, L. & Hoepfner, M. P. Molecular polydispersity improves prediction of asphaltene aggregation. *J. Mol. Lig.* **256**, 382–394 (2018).
- 46. Zhang, Y. Identify Similarities in Diverse Polycyclic Aromatic Hydrocarbons of Asphaltenes and Heavy Oils Revealed by Noncontact Atomic Force Microscopy: Aromaticity, Bonding, and Implications in Reactivity. ACS Symp. Ser. 1320, 39–65 (2019).
- 47. Zhang, Y., Schuler, B., Fatayer, S., Gross, L., Harper, M. R. & Kushnerick, J. D. Understanding the Effects of Sample Preparation on the Chemical Structures of Petroleum Imaged with Noncontact Atomic Force Microscopy. *Ind. Eng. Chem. Res.* **57**, 15935–15941 (2018).
- 48. Chaisoontornyotin, W., Yang, Y. & Hoepfner, M. P. Studies on the Kinetic Precipitation of Asphaltenes in Athabasca Bitumen. PhD Dissertation, University of Utah, Department of Chemical

- Engineering (2017).
- 49. Bowron, D. T. *et al.* NIMROD: The Near and InterMediate Range Order Diffractometer of the ISIS second target station. *Rev. Sci. Instrum.* **81**, 033905 (2010).
- 50. Lindner, P. (Peter) & Zemb, T. (Thomas). Neutrons, X-rays, and light: scattering methods applied to soft condensed matter. (Elsevier, 2002).
- 51. Sivia, D. S. Elementary Scattering Theory: For X-ray and Neutron Users. in *Elementary Scattering Theory: For X-ray and Neutron Users* (2011).
- 52. Fischer, H. E., Barnes, A. C. & Salmon, P. S. Neutron and x-ray diffraction studies of liquids and glasses. *Reports Prog. Phys.* **69**, 233 (2006).
- 53. Hammouda, B. A new Guinier-Porod model. J. Appl. Crystallogr. 43, 716-719 (2010).
- 54. Barré, L., Simon, S. & Palermo, T. Solution Properties of Asphaltenes. *Langmuir* **24**, 3709–3717 (2008).
- 55. Soper, A. K. Inelasticity corrections for time-of-flight and fixed wavelength neutron diffraction experiments. *Mol. Phys.* **107**, 1667–1684 (2009).
- 56. Temleitner, L., Stunault, A., Cuello, G. J. & Pusztai, L. Neutron diffraction of hydrogenous materials: Measuring incoherent and coherent intensities separately from liquid water a 40-year-old puzzle solved. *Phys. Rev. B Condens. Matter Mater. Phys.* **92**, 1–8 (2015).
- 57. Soper, A. K. GudrunN and GudrunX: Programs for Correcting Raw Neutron and X-ray Diffraction Data to Differential Scattering Cross Section. RAL Report RAL-TR-2011-013 http://purl.org/net/epubs/work/56240 (2011).
- 58. Sirota, E. B. Swelling of Asphaltenes. *Pet. Sci. Technol.* **16**, 415–431 (1998).
- 59. Ingham, B. & Toney, M. F. X-ray diffraction for characterizing metallic films. in *Metallic Films* for Electronic, Optical and Magnetic Applications: Structure, Processing and Properties 3–38 (Woodhead Publishing, 2013). doi:10.1533/9780857096296.1.3.

- 60. Calvin, S., Luo, S. X., Caragianis-Broadbridge, C., McGuinness, J. K., Anderson, E., Lehman, A., Wee, K. H., Morrison, S. A. & Kurihara, L. K. Comparison of extended x-ray absorption fine structure and Scherrer analysis of x-ray diffraction as methods for determining mean sizes of polydisperse nanoparticles. *Appl. Phys. Lett.* 87, 1–3 (2005).
- 61. Scherrer, P. Bestimmung der inneren Struktur und der Größe von Kolloidteilchen mittels Röntgenstrahlen. in *Kolloidchemie Ein Lehrbuch* 387–409 (1912). doi:10.1007/978-3-662-33915-2_7.
- 62. Mittemeijer, E. J. & Welzel, U. The 'state of the art' of the diffraction analysis of crystallite size and lattice strain. in *Zeitschrift fur Kristallographie* vol. 223 552–560 (2008).
- 63. Thiyagarajan, P., Hunt, J. E., Winans, R. E., Anderson, K. B. & Miller, J. T. Temperature-Dependent Structural Changes of Asphaltenes in 1-Methylnaphthalene. *Energy & Fuels* **9**, 829–833 (1995).
- 64. Larson, R. G. The Structure and Rheology of Complex Fluids. (Oxford University Press, 1999).
- 65. Yang, X., Hamza, H. & Czarnecki, J. Investigation of subfractions of Athabasca asphaltenes and their role in emulsion stability. *Energy and Fuels* **18**, 770–777 (2004).
- 66. Verruto, V. J. & Kilpatrick, P. K. Preferential Solvent Partitioning within Asphaltenic Aggregates Dissolved in Binary Solvent Mixtures. *Energy & Fuels* **21**, 1217–1225 (2007).
- 67. Evdokimov, I. N., Eliseev, N. Y. & Akhmetov, B. R. Asphaltene dispersions in dilute oil solutions. *Fuel* **85**, 1465–1472 (2006).
- 68. Gray, M. R., Tykwinski, R. R., Stryker, J. M. & Tan, X. Supramolecular Assembly Model for Aggregation of Petroleum Asphaltenes. *Energy & Fuels* **25**, 3125–3134 (2011).
- 69. Pfeiffer, J. P. & Saal, R. N. J. Asphaltic Bitumen as Colloid System. *J. Phys. Chem.* 44, 139–149 (1940).
- 70. Placzek, G. & Van Hove, L. Crystal dynamics and inelastic scattering of neutrons. Phys. Rev. 93,

- 1207-1214 (1954).
- 71. Zhao, K. & Mason, T. G. Assembly of colloidal particles in solution. *Reports Prog. Phys.* 81, 126601 (2018).
- 72. Taylor, S. L., Evans, R. & Patrick Royall, C. Temperature as an external field for colloid-polymer mixtures: 'Quenching' by heating and 'melting' by cooling. *J. Phys. Condens. Matter* **24**, 8 (2012).
- 73. Zhao, K. & Mason, T. G. Directing Colloidal Self-Assembly through Roughness-Controlled Depletion Attractions. *Phys. Rev. Lett.* **99**, 268301 (2007).
- 74. Goual, L., Sedghi, M., Mostowfi, F., McFarlane, R., Pomerantz, A. E., Saraji, S. & Mullins, O. C. Cluster of Asphaltene Nanoaggregates by DC Conductivity and Centrifugation. *Energy & Fuels* 28, 5002–5013 (2014).
- 75. Smith, J. M., Van Ness, H. C. & Abbott, M. M. Introduction to Chemical Engineering Thermodynamics. (McGraw-Hill, 2005).
- 76. Holzhauer, J. K. & Ziegler, W. T. Temperature dependence of excess thermodynamic properties of n-heptane-toluene, methylcyclohexane-toluene, and n-heptane-methylcyclohexane systems. *J. Phys. Chem.* **79**, 590–604 (1975).
- 77. Marshall, A. G. & Rodgers, R. P. Petroleomics: Chemistry of the underworld. *Proc. Natl. Acad. Sci.* **105**, 18090–18095 (2008).
- Headen, T. F., Howard, C. A., Skipper, N. T., Wilkinson, M. A., Bowron, D. T. & Soper, A. K.
 Structure of π-π Interactions in Aromatic Liquids. J. Am. Chem. Soc. 132, 5735–5742 (2010).
- 79. Falkowska, M., Bowron, D. T., Manyar, H. G., Hardacre, C. & Youngs, T. G. A. Neutron Scattering of Aromatic and Aliphatic Liquids. *Chemphyschem* 17, 2043–2055 (2016).
- 80. Yang, Y., Chaisoontornyotin, W. & Hoepfner, M. P. Structure of Asphaltenes during Precipitation Investigated by Ultra-Small-Angle X-ray Scattering. *Langmuir* **34**, (2018).

81. Headen, T. F. & Hoepfner, M. P. Structural insights into crude oil asphaltenes: A multi-parametric SANS/WANS study. *STFC ISIS Neutron Muon Source* (2017) doi:doi.org/10.5286/ISIS.E.RB1710282.

TOC Graphic:

